

Properties of QCD axion in two-flavor color superconductive matter with massive quarks

Zhao Zhang* and Wenhao Zhao

School of Mathematics and Physics, North China Electric Power University, Beijing 102206, China

We investigate the properties of QCD axion at low temperature and moderate density in the Nambu-Jona-Lasinio model with instanton induced interactions by simultaneously considering the scalar and pseudo-scalar condensates in both quark-antiquark and diquark channels. We derive the analytical dispersion relations of quarks with four-type condensates at nonzero theta angle $\theta = a/f_a$. The axion mass, quadratic self-coupling, and the axion potential are calculated in both the chiral symmetry broken and two-flavor color superconductive phases. Using the commonly adopted model parameters, we find that due to the emergence of color superconductivity, the chiral phase transition not only does not lead to a significant decrease in axion mass and self-coupling, but rather results in an obvious enhancement of them. As a θ function, the axion potential exhibits an appropriate period of π , which is quite different from the case without considering the color superconductivity. The surface tension of axion domain wall is also calculated in the presence of color superconductivity.

I. INTRODUCTION

The complicated nature of the QCD vacuum reveals that the effective Lagrangian should include an extra term

$$\mathcal{L}_{\theta_0} = \theta_0 \frac{g^2}{32\pi^2} G_{\mu\nu}^a \cdot \tilde{G}^{a\mu\nu} = \theta_0 Q \quad (1)$$

where $G_{\mu\nu}^a$ and $\tilde{G}^{a\mu\nu}$ denote the gluon field strength tensor and its dual respectively, while Q is the topological charge density and θ_0 is a real parameter. This term breaks both parity and time reversal symmetry but respects charge conjugation symmetry. Considering the quark mass matrix M_q , the complete coefficient of Q reads

$$\theta = \theta_0 - \arg(\det M_q). \quad (2)$$

The phase angle θ is directly related to the neutron electric dipole moment (NEDM) d_n via the predicted relation

$$|d_n| \sim 10^{-16} \theta e \cdot cm \quad (3)$$

in the standard model [1]. The experiment limit on the NEDM [2, 3] suggests $\theta < 2 \times 10^{-10}$. The extremely small θ indicates the CP (charge conjugation and parity) symmetry is conserved in strong interaction. This creates the so called fine-tuning or strong CP problem: the two sources of θ cancel with such precision is unnatural since they have distinct origins (one is related to the QCD vacuum and the other the Higgs mechanism).

The Peccei-Quinn(PQ) mechanism is the most compelling solution to the strong CP problem which involves an extra $U(1)$ chiral symmetry beyond the standard model [4, 5]. The QCD axion is the pseudo-Nambu-Goldstone boson arising from the spontaneously breaking of $U(1)_{PQ}$ symmetry [6, 7] which may occur at

the energy scale indicated by the axion decay constant f_a . The axion mass, self coupling, and couplings to other particles are all inversely proportional to f_a . Experimental constraints suggest that f_a must be much higher than the electroweak breaking scale [8]. This implies QCD axion is a very weakly interacting particle with a small mass and thus is invisible [9–12]. These properties make the axion one of the leading candidates for dark matter [13–16].

Besides QCD axion, the axion-like particles (ALP) are also proposed as the promising dark matter candidates [17, 18]. As extremely light bosons, QCD axions and ALPs may form stars as well as the Bose-Einstein condensates [19–36]. The axions might be produced copiously in the interiors of stellar objects via the Primakoff process, the Compton-like process, axion bremsstrahlung, etc [37]. As a light and feebly interacting particle, the axion may influence the energy budget of stars drastically and affect the stellar evolution: axions may transport the energy of stars to outer space and shorten the star lifetime [38–45]. Moreover, a recent work has shown that the axion cloud may form around the neutron stars [46]. Since we only study QCD axion in this paper, we refer to QCD axion as axion for convenience in the following.

To understand the axion roles in cosmology and astrophysics, we must know the axion properties, e.g., axion mass, self-coupling, and couplings to normal matter in the hot and dense medium. The dependences of axion properties on the temperature and fermion chemical potentials determine how the axion affects the formation of large-scale structure of the universe, the cosmological evolution, and the properties and evolutions of stellar objects. In this work, we mainly concentrate on how the axion potential, axion mass and self-coupling change when QCD phase transitions happen at finite temperature and baryon density.

Most of properties of the axion are determined by the non-perturbative QCD dynamics. In the literatures, the axion mass and quadratic self-coupling in cool and hot medium had been studied using lattice QCD(LQCD) [47–

* zhaozhang@pku.org.cn

51] and chiral perturbation theory(χ PT) [52]. However, applying LQCD in dense medium has the limitation due to the sign problem and χ PT fails to describe QCD phase transitions (due to the lack of quark degrees of freedom). So to investigate the impact of QCD phase transitions on axion properties in dense medium, one must resort to other methods, such as the low energy effective theories and models. Nambu-Jona-Lasinio (NJL) model [53, 54] is an extensively used formalism for the study of QCD phase diagram [55–57]. Recently, this model has been adopted to study the low energy properties of axion in the hot and dense quark matter without considering the possible Cooper pairings [58–61].

Note that the color superconducting quark matter [62–66] may appear in the cores of compact stars. Thus it is interesting to explore how the axion is influenced by the diquark condensates in phases of color superconductivity (CS). Recent studies on this topic can be found in Refs.[67, 68]. For asymptotically large baryon density, axion properties in the color flavor locking (CFL) phase [64] was calculated by employing a chiral effective theory in [67]. For moderate baryon density, the coupling of the axion to two flavor color superconductivity (2CS) was investigated within a NJL-type model in [68], where both scalar and pseudo-scalar diquark condensates are considered via the instanton induced interactions. However, the chiral condensate and its pseudo-scalar partner, which may play important roles near the phase boundary between the chiral symmetry broken and CS phases, are all missed in [67, 68].

In the region of low temperature and intermediate quark chemical potential, there may exist competition between the chiral and diquark condensates [66]. Especially, the nontrivial interplay between these two types of condensates may weaken the chiral transition at low temperatures and lead to multiple critical end points [69–72]. In order to obtain a complete insight on the in-medium properties of axion from the whole picture of the T - μ phase diagram of QCD, one must take into account the condensates related to Dirac-type masses in the presence of CS. The motivation of this work is to study the low energy properties of axion in dense medium by simultaneously including the couplings among the axion, quark-antiquark condensates, and diquark condensates. To do this, we adopt the two flavor NJL model with the one-gluon and singel-instanton exchange interactions in both the meson-meson and diquark-diquark channels. We mainly focus on the axion potential, axion mass, axion self coupling, and axion domain wall structure at moderate baryon density.

The rest of this paper is organized as follows. In section II, we describe the formalism which can simultaneously address the couplings between the axion field and two types of effective masses: the Dirac-type masses related to quark-antiquark condensates as well as the Majorana-type masses related to diquark condensates. In section III, we show the numerical results. The conclusion and discussion are presented in section IV.

II. THE FORMALISM

In this section, we present how to simultaneously consider the couplings among the axion field and the scalar and pseudo-scalar condensates in both the quark-antiquark and diquark channels at the mean field level in the framework of two-flavor NJL model of QCD.

A. Lagrangian of a two-flavor NJL with instanton induced interactions

There are many variants of NJL-type model [55–57]. In this study, we adopt a formalism of two flavor NJL model with two types of local four-quark interactions.

The first is the color current interaction arises from the one-gluon exchange, which takes the form

$$\mathcal{L}_{\text{int1}} = -g_1(\bar{q}\gamma_\mu\lambda_a q)^2, \quad (4)$$

where λ_a denote the Gell-Mann matrixes in color space and g_1 is the coupling constant. This interaction respects the global $U(2)_V \otimes U(2)_A$ symmetry in the two flavor case. The Fierz transformation of $\mathcal{L}_{\text{int1}}$ can give rise to different interaction forms in both the quark-antiquark and diquark channels (see Ref.[57] for details). Here, we only consider the scalar and pseudo-scalar quark-antiquark and diquark channels, namely

$$\mathcal{L}_{\text{qq1}} = G_1 [(\bar{q}q)^2 + (\bar{q}i\gamma_5 q)^2 + (\bar{q}\vec{\tau}q)^2 + (\bar{q}i\gamma_5 \vec{\tau}q)^2] \quad (5)$$

with $G_1 = \frac{N_c^2 - 1}{N_c^2} g_1$ and

$$\mathcal{L}_{\text{qq1}} = H_1 \sum_A [(q^T C i\gamma_5 \tau_2 \lambda_A q) (\bar{q}i\gamma_5 C \tau_2 \lambda_A \bar{q}^T) + (q^T C \tau_2 \lambda_A q) (\bar{q}C \tau_2 \lambda_A \bar{q}^T)] \quad (6)$$

with $H_1 = \frac{N_c + 1}{2N_c} g_1$, where $N_c = 3$ is the color number and λ_A ($A=2,5,7$) are the antisymmetric Gell-Mann matrixes in color space. The τ_a in Eqs.(5) and (6) are Pauli matrixes in flavor space and $C = i\gamma^2\gamma^0$ is the charge conjugate matrix. Note that only the flavor and color antisymmetric diquark channels are listed in Eq.(6). We see that the standard ratio H_1/G_1 in the Fierz transformation is 3/4 for $N_c = 3$.

Another one is the singe instanton induced four-quark interaction for the two flavor case, which reads

$$\mathcal{L}_{\text{int2}} = \frac{g_2}{4(N_c^2 - 1)} \left\{ \frac{2N_c - 1}{2N_c} \times [(\bar{q}q)^2 - (\bar{q}i\gamma_5 q)^2 - (\bar{q}\tau_a q)^2 + (\bar{q}\tau_a i\gamma_5 q)^2] - \frac{1}{4N_c} [(\bar{q}\sigma^{\mu\nu} q)^2 - (\bar{q}\sigma^{\mu\nu} \tau_a q)^2] \right\} \quad (7)$$

according to Ref.[65]. This interaction respects the global $U(1)_V \otimes SU(2)_V \otimes SU(2)_A$ symmetry but violates the global $U(1)_A$ symmetry explicitly, which is usually used

to describe the axial anomaly of QCD in the NJL-type models. Performing the Feirz transformation of $\mathcal{L}_{\text{int2}}$, we obtain the scalar and pseudo-scalar quark-antiquark interactions

$$\mathcal{L}_{q\bar{q}2} = G_2 [(\bar{q}q)^2 - (\bar{q}i\gamma_5 q)^2 - (\bar{q}\vec{\tau}q)^2 + (\bar{q}i\gamma_5 \vec{\tau}q)^2] \quad (8)$$

and the scalar and pseudo-scalar diquark interactions

$$\begin{aligned} \mathcal{L}_{qq2} = H_2 \sum_A & [(q^T C i\gamma_5 \tau_2 \lambda_A q)(\bar{q}i\gamma_5 C \tau_2 \lambda_A \bar{q}^T) \\ & - (q^T C \tau_2 \lambda_A q)(\bar{q}C \tau_2 \lambda_A \bar{q}^T)], \end{aligned} \quad (9)$$

where $G_2 = \frac{g_2}{4N_c^2}$ and $H_2 = \frac{g_2}{8N_c(N_c-1)}$ [57, 65]. Similar to \mathcal{L}_{qq1} , the color and flavor symmetric diquark channels are ignored in \mathcal{L}_{qq2} . The Feirz transformation also gives rise to the ratio $H_2/G_2 = 3/4$ for $N_c = 3$.

As mentioned, we will simultaneously take into account the scalar and pseudo-scalar condensates in both the quark-antiquark and diquark channels. We adopt the following Lagrangian density

$$\mathcal{L} = \bar{q}(i\partial + \hat{\mu}\gamma_0 - m_0)q + \mathcal{L}_{q\bar{q}} + \mathcal{L}_{qq}, \quad (10)$$

where

$$\mathcal{L}_{q\bar{q}} = \mathcal{L}_{q\bar{q}1} + \mathcal{L}_{q\bar{q}2}, \quad (11)$$

and

$$\mathcal{L}_{qq} = \mathcal{L}_{qq1} + \mathcal{L}_{qq2}. \quad (12)$$

Note that in Ref.[68], only the diquark interaction (12) is taken into account and the quark masses are ignored for simplicity.

We use the coupling constant G and a dimensionless parameter c to indicate the couplings G_1 and G_2 through the relations

$$G_2 = cG, \quad G_1 = (1-c)G. \quad (13)$$

The parameter G can be fixed by the vacuum properties of QCD.

B. Lagrangian of NJL with axion field

To introduce the axial field conveniently, it is more useful to express the Lagrangian density (10) in term of the left(right)-handed quark field $q_{L(R)} = \mathcal{P}_{L(R)}q$, where

$$\mathcal{P}_R = \frac{1 + \gamma_5}{2}, \quad \mathcal{P}_L = \frac{1 - \gamma_5}{2}. \quad (14)$$

Using $q_{L(R)}$, the interaction $\mathcal{L}_{q\bar{q}2}$ can be rewritten as the sum of two determinants

$$\mathcal{L}_{q\bar{q}2} = 8G_2 [\det(\bar{q}_R q_L) + \det(\bar{q}_L q_R)], \quad (15)$$

and the diquark interaction \mathcal{L}_{qq2} takes the form

$$\mathcal{L}_{qq2} = -2H_2 \sum_A [d_{A,R}^\dagger d_{A,L} + d_{A,L}^\dagger d_{A,R}], \quad (16)$$

where

$$d_{A,L(R)} = q_{L(R)}^T C i\tau_2 \lambda_A q_{L(R)}. \quad (17)$$

Performing the following $U(1)_A$ transformation

$$q_L \rightarrow e^{-i\alpha} q_L \text{ and } q_R \rightarrow e^{i\alpha} q_R, \quad (18)$$

the interactions $\mathcal{L}_{q\bar{q}2}$ and \mathcal{L}_{qq2} become

$$\mathcal{L}_{q\bar{q}2} \rightarrow 8G_2 [e^{-i4\alpha} \det(\bar{q}_R q_L) + e^{i4\alpha} \det(\bar{q}_L q_R)] \quad (19)$$

and

$$\mathcal{L}_{qq2} \rightarrow -2H_2 \sum_A [e^{-i4\alpha} d_{A,R}^\dagger d_{A,L} + e^{i4\alpha} d_{A,L}^\dagger d_{A,R}], \quad (20)$$

respectively. The axion field is then introduced by replacing the phase factor 4α (namely $2N_f\alpha$ for $N_f = 2$) in Eqs.(19) and (20) with a/f_a , where a is the axion field. So the NJL lagrangian density with the axion field takes the form

$$\begin{aligned} \mathcal{L}_{\text{eff}} = & \bar{q}(i\partial + \hat{\mu}\gamma_0 - m_0)q \\ & + \mathcal{L}_{q\bar{q}1} + \mathcal{L}_{qq1} + \mathcal{L}_{aq\bar{q}} + \mathcal{L}_{aqq}, \end{aligned} \quad (21)$$

where

$$\mathcal{L}_{aq\bar{q}} = 8G_2 [e^{-i\frac{a}{f_a}} \det(\bar{q}_R q_L) + e^{i\frac{a}{f_a}} \det(\bar{q}_L q_R)] \quad (22)$$

and

$$\mathcal{L}_{aqq} = -2H_2 \sum_A [e^{-i\frac{a}{f_a}} d_{A,R}^\dagger d_{A,L} + e^{i\frac{a}{f_a}} d_{A,L}^\dagger d_{A,R}] \quad (23)$$

We can rewrite the interaction \mathcal{L}_{aqq} as

$$\begin{aligned} \mathcal{L}_{aqq} = & H_2 \sum_A [(\bar{q}i\gamma_5 C \tau_2 \lambda_A \bar{q}^T)(q^T C i\gamma_5 \tau_2 \lambda_A q) \cos(\frac{a}{f_a}) \\ & - (\bar{q}i\gamma_5 C \tau_2 \lambda_A \bar{q}^T)(q^T C \tau_2 \lambda_A q) \sin(\frac{a}{f_a}) \\ & - (\bar{q}C \tau_2 \lambda_A \bar{q}^T)(q^T C i\gamma_5 \tau_2 \lambda_A q) \sin(\frac{a}{f_a}) \\ & + (\bar{q}C i\tau_2 \lambda_A \bar{q}^T)(q^T C i\tau_2 \lambda_A q) \cos(\frac{a}{f_a})]. \end{aligned} \quad (24)$$

Note that the diquark interaction \mathcal{L}_{qq1} can also be written in term of $d_{A,R}$ and $d_{A,L}$, which reads

$$\mathcal{L}_{qq1} = 2H_1 \sum_A [d_{A,R}^\dagger d_{A,R} + d_{A,L}^\dagger d_{A,L}]. \quad (25)$$

Clearly this interaction is $U(1)_A$ -preserving and thus doesn't couple with the axion field.

C. Nambu-Gorkov propagator with quark-antiquark and diquark condensates

For nonzero $\theta = a/f_a$, four condensates, namely the chiral condensate σ , the pseudo-scalar quark condensate η , the scalar diquark condensate δ , and the pseudo-scalar diquark condensate ω , may appear at low temperature and moderate density. These condensates are defined as

$$\langle \bar{q}q \rangle = \sigma, \quad (26)$$

$$\langle \bar{q}i\gamma_5 q \rangle = \eta, \quad (27)$$

$$\langle q^T C i\gamma_5 \tau_2 \lambda_2 q \rangle = \delta, \quad (28)$$

$$\langle \bar{q}i\gamma_5 \tau_2 \lambda_2 C \bar{q}^T \rangle = \delta^*, \quad (29)$$

$$\langle q^T C i\tau_2 \lambda_2 q \rangle = \omega, \quad (30)$$

$$\langle \bar{q}i\tau_2 \lambda_2 C \bar{q}^T \rangle = -\omega^*. \quad (31)$$

Following the convention, red and green quarks are assumed to participate the Cooper pairing and thus only λ_2 appears in Eqs.(28)-(31). We can define the following left and right handed diquark condensates

$$\langle d_{2,L} \rangle = \langle q_L^T C i\tau_2 \lambda_2 q_L \rangle = h_L, \quad (32)$$

$$\langle d_{2,L}^\dagger \rangle = -\langle \bar{q}_L C i\tau_2 \lambda_2 \bar{q}_L^T \rangle = h_L^*, \quad (33)$$

$$\langle d_{2,R} \rangle = \langle q_R^T C i\tau_2 \lambda_2 q_R \rangle = h_R. \quad (34)$$

$$\langle d_{2,R}^\dagger \rangle = -\langle \bar{q}_R C i\tau_2 \lambda_2 \bar{q}_R^T \rangle = h_R^*. \quad (35)$$

Clearly, there exists the relations

$$\begin{aligned} \delta &= h_R - h_L, & \omega &= h_L + h_R \\ \delta^* &= h_R^* - h_L^*, & \omega^* &= h_L^* + h_R^*. \end{aligned} \quad (36)$$

Note that $h_{L(R)}$ introduced above corresponds to $-h_{L(R)}$ used in [68]. Since both τ_2 and λ_2 in Eqs.(32)-(35) are imaginary matrixes, the relation (36) is still the same as that in [68].

We will adopt the mean field treatment in this paper. Using the assumptions $\delta = \delta^*$ and $\omega = \omega^*$ (or $h_L = h_L^*$ and $h_R = h_R^*$ as that in [68].), we get the following mean field Lagrangian related to the diquark couplings H_1 and H_2

$$\begin{aligned} \mathcal{L}_{\text{Mqq}} = & H_1 [\delta(\bar{q}i\gamma_5 C \tau_2 \lambda_2 \bar{q}^T) + \delta^*(q^T C i\gamma_5 \tau_2 \lambda_2 q)] \\ & - H_1 [\omega(\bar{q}iC \tau_2 \lambda_2 \bar{q}^T) - \omega^*(q^T iC \tau_2 \lambda_2 q)] \\ & + H_2 [\delta(\bar{q}i\gamma_5 C \tau_2 \lambda_2 \bar{q}^T) + \delta^*(q^T C i\gamma_5 \tau_2 \lambda_2 q)] \cos \frac{a}{f_a} \\ & + H_2 [-\delta^*(q^T C \tau_2 \lambda_A q) - \omega(\bar{q}\gamma_5 C \tau_2 \lambda_A \bar{q}^T)] \sin \frac{a}{f_a} \\ & + H_2 [-\delta(\bar{q}C \tau_2 \lambda_A \bar{q}^T) + \omega^*(q^T C \gamma_5 \tau_2 \lambda_A q)] \sin \frac{a}{f_a} \\ & + H_2 [\omega(\bar{q}C i\tau_2 \lambda_A \bar{q}^T) - \omega^*(q^T C i\tau_2 \lambda_A q)] \cos \frac{a}{f_a} \\ & - H_1 [|\delta|^2 + |\omega|^2] - H_2 [|\delta|^2 - |\omega|^2] \cos \frac{a}{f_a}. \end{aligned} \quad (37)$$

The mean field interaction Lagrangian related to G_1 and G_2 is the same as that in [58].

To study the quark Cooper pairings, it is more convenient to use the Nambu-Gorkov formalism [57]. So we introduce the following bi-spinors of quark fields

$$\Psi = \begin{pmatrix} \frac{1}{\sqrt{2}}q \\ \frac{1}{\sqrt{2}}C\bar{q}^T \end{pmatrix}, \quad \bar{\Psi} = \begin{pmatrix} 1 \\ \frac{1}{\sqrt{2}}\bar{q} \\ \frac{1}{\sqrt{2}}q^T C \end{pmatrix}. \quad (38)$$

The interaction Lagrangian density with the axial field at the mean field level is then rewritten as

$$\mathcal{L} = \bar{\Psi} S^{-1} \Psi - \mathcal{V}, \quad (39)$$

where S^{-1} is the inverse Nambu-Gorkov quark propagator and

$$\begin{aligned} \mathcal{V} = & G_1 (\eta^2 + \sigma^2) - G_2 (\eta^2 - \sigma^2) \cos \frac{a}{f_a} + 2G_2 \sigma \eta \sin \frac{a}{f_a} \\ & + H_1 (\delta^2 + \omega^2) + H_2 (\delta^2 - \omega^2) \cos \frac{a}{f_a}. \end{aligned} \quad (40)$$

In the presence of the condensates σ , η , δ , and ω , the matrix S^{-1} in the momentum space takes the form

$$S^{-1}(p) = \begin{pmatrix} (\not{p}_+ - M) \mathbf{1}_C \mathbf{1}_F & \Phi^- \\ \Phi^+ & (\not{p}_- - M) \mathbf{1}_C \mathbf{1}_F \end{pmatrix}, \quad (41)$$

where

$$\not{p}_\pm = \not{p} \pm \mu \gamma_0, \quad (42)$$

$$M = M_s - i\gamma_5 M_p, \quad (43)$$

$$\Phi^- = \Delta_s [i\gamma_5 \tau_2 \lambda_2] + \Delta_p \tau_2 \lambda_2, \quad (44)$$

$$\Phi^+ = \Delta_s^* [i\gamma_5 \tau_2 \lambda_2] + \Delta_p^* \tau_2 \lambda_2, \quad (45)$$

and $\mathbf{1}_C(F)$ is the identity matrix in color (flavor) space.

Four energy gaps appear in Eqs.(43)-(45), namely the scalar (pseudo-scalar) Dirac-type mass $M_s(M_p)$ and the scalar (pseudo-scalar) Majorana-type mass $\Delta_s(\Delta_p)$, which are defined as

$$M_s = m_0 - 2 \left(G_1 + G_2 \cos \frac{a}{f_a} \right) \sigma - 2G_2 \eta \sin \frac{a}{f_a} \quad (46)$$

$$M_p = -2 \left(G_1 - G_2 \cos \frac{a}{f_a} \right) \eta - 2G_2 \sigma \sin \frac{a}{f_a}, \quad (47)$$

$$\Delta_s = (2H_1 + 2H_2 \cos \frac{a}{f_a}) \delta + i2H_2 \omega \sin \frac{a}{f_a}, \quad (48)$$

$$\Delta_p = -2H_2 \delta \sin \frac{a}{f_a} - i(2H_1 - 2H_2 \cos \frac{a}{f_a}) \omega. \quad (49)$$

Unlike M_s and M_p , we see that Δ_s and Δ_p are complex quantities for nonzero axion field.

D. Thermodynamic potential

As in the previous studies [58, 68], the axion field is treated as a classical background here. Performing the standard functional integration over the quark fields, we

can obtain the mean field thermodynamical potential at a fixed a/f_a , which reads

$$\Omega = \mathcal{V} + \Omega_q, \quad (50)$$

where

$$\Omega_q = -T \sum_n \int \frac{d^3 p}{(2\pi)^3} \frac{1}{2} \text{Tr} \ln \left(\frac{1}{T} S^{-1}(i\omega_n, \vec{p}) \right) \quad (51)$$

is the one-loop contribution of the fermions. In (51), $w_n = (2n+1)\pi T$ are the Matsubara frequencies for fermions in the imaginary time thermal field theory and the trace is taken over the Nambu-Gorkov, Dirac, color, and flavor spaces. The added overall factor 1/2 is used to cancel the doubling of degrees of freedom due to the use of bi-spinors [57].

The Matsubara summation in (51) can be simplified significantly once we obtain the eigenvalues of the following matrix (for more details on the method see the appendix of Ref. [73] or [74]).

$$\mathcal{Z} = \gamma^0 S^{-1}(p_0, \vec{p}) - p_0 \mathbf{1} \quad (52)$$

$$= \begin{pmatrix} -\vec{\gamma} \cdot \vec{p} + \mu - \gamma^0 M & \gamma^0 \Phi^- \\ \gamma^0 \Phi^+ & -\vec{\gamma} \cdot \vec{p} - \mu - \gamma^0 M \end{pmatrix} \quad (53)$$

The traceless property of this matrix indicates that if E_i is its eigenvalue then $-E_i$ may also be, which has been confirmed in our calculation. Even the matrix \mathcal{Z} is more complicated than the corresponding one without the mass M in [68], we can still get the analytical eigenvalues which read

$$E_{1,\pm} = \pm \sqrt{(E - \mu)^2} = \pm \epsilon_1(\vec{p}), \quad (54)$$

$$E_{2,\pm} = \pm \sqrt{(E + \mu)^2} = \pm \epsilon_2(\vec{p}), \quad (55)$$

$$E_{3,\pm} = \pm \sqrt{E'^2 + \mu^2 - Z_+^2} = \pm \epsilon_3(\vec{p}), \quad (56)$$

$$E_{4,\pm} = \pm \sqrt{E'^2 + \mu^2 + Z_+^2} = \pm \epsilon_4(\vec{p}), \quad (57)$$

$$E_{5,\pm} = \pm \sqrt{E'^2 + \mu^2 - Z_-^2} = \pm \epsilon_5(\vec{p}), \quad (58)$$

$$E_{6,\pm} = \pm \sqrt{E'^2 + \mu^2 + Z_-^2} = \pm \epsilon_6(\vec{p}), \quad (59)$$

where

$$E = \sqrt{p^2 + M_s^2 + M_p^2} \quad (60)$$

$$E'^2 = p^2 + M_s^2 + M_p^2 + |\Delta_s|^2 + |\Delta_p|^2 \quad (61)$$

and $p = |\vec{p}|$. The terms Z_{\pm}^2 reflect the mixing between the Dirac and Majorana masses which are defined as

$$Z_{\pm}^2 = \{ [|\Delta_s^* \Delta_p - \Delta_s \Delta_p^*| \pm 2p\mu]^2 + 4[|\Delta_s|^2 M_p^2 + |\Delta_p|^2 M_s^2 + M^2 \mu^2 - M_s M_p (\Delta_s^* \Delta_p + \Delta_s \Delta_p^*)] \}^{1/2}, \quad (62)$$

where

$$|\Delta_s^* \Delta_p - \Delta_s \Delta_p^*| = 8(H_1^2 - H_2^2)\delta\omega. \quad (63)$$

Since the inverse Nambu-Gokov propagator is a 48×48 matrix, only twelve independent eigenvalues displayed in (54)-(59) imply that the multiplicity of each eigenvalue equals to four.

We see that eigenvalues $E_{1,\pm}$ and $E_{2,\pm}$ only depend on the Dirac masses but the ones from $E_{3,\pm}$ to $E_{6,\pm}$ depend both on the Dirac and Majorana masses. Clearly, the former corresponds to the dispersion relations of the blue quarks and the later the red and green ones. We can check that for vanishing M_s and M_p , Eqs.(54)-(59) can be reduced to the corresponding dispersion relations obtained in [68] where only the Majorana masses are considered. On the other hand, the standard quark dispersion relations for 2CS [66] can be reproduced from Eqs.(54)-(59) by fixing $a/f_a = 0$ (and thus $M_p = \Delta_p = 0$).

Using the identity

$$\text{Tr} \ln \frac{1}{T} S^{-1} = \ln \det \frac{1}{T} S^{-1},$$

we can decompose the trace in (51) as

$$\text{Tr} \ln \frac{1}{T} S^{-1}(i\omega_n, \vec{p}) = 4 \sum_{k=1}^6 \ln \left(\frac{\omega_n^2 + \epsilon_k(\vec{p})^2}{T^2} \right), \quad (64)$$

where ϵ_k are the six independent positive eigenvalues listed in Eqs.(54)-(59) and the factor four in the RHS of (64) is the eigenvalue degeneracy. Now the Matsubara summation (51) can be evaluated analytically by employing the standard relation [75]

$$\sum_n \ln \left(\frac{\omega_n^2 + \varepsilon^2}{T^2} \right) = \frac{|\varepsilon|}{T} + 2 \ln \left(1 + e^{-|\varepsilon|/T} \right). \quad (65)$$

We then obtain the following mean field thermodynamic potential

$$\Omega = -2 \sum_{k=1}^6 \int \frac{d^3 p}{(2\pi)^3} \left[\epsilon_k(\vec{p}) + 2T \ln \left(1 + e^{-\epsilon_k(\vec{p})/T} \right) \right] + \mathcal{V}. \quad (66)$$

For a given value of a/f_a at fixed T and μ , the thermodynamical potential is a function of σ , η , δ , and ω . The physical value of these condensates are determined by the following gap equations

$$\frac{\partial \Omega}{\partial \sigma} = 0, \quad \frac{\partial \Omega}{\partial \eta} = 0, \quad \frac{\partial \Omega}{\partial \delta} = 0, \quad \frac{\partial \Omega}{\partial \omega} = 0. \quad (67)$$

E. Axion potential, axion mass, and self-coupling

The effective axion potential can be defined as

$$V(a, T, \mu) = \Omega(x_i(a, T, \mu), a, T, \mu), \quad (68)$$

where $x_i(a, T, \mu)$ refer to the physical values of the aforementioned four condensates obtained at given a , T , and μ .

By taking the second derivative of the potential (68) with respect to a at $a = 0$, we can obtain the axion mass squared

$$m_a^2 = \frac{d^2 V}{da^2} \Big|_{a=0} = \frac{\chi_t}{f_a^2}, \quad (69)$$

where χ_t is the topological susceptibility. The axion quadratic self-coupling is defined as the fourth derivative of (68) at $a = 0$, which reads

$$\lambda_a = \frac{d^4 V}{da^4} \Big|_{a=0}. \quad (70)$$

Since the physical condensates are all implicitly dependent on a , the total differential of $V(a)$ with respect to a satisfies the following relation

$$\frac{dV}{da} = \frac{\partial V}{\partial a} + \frac{\partial V}{\partial \sigma} \frac{\partial \sigma}{\partial a} + \frac{\partial V}{\partial \eta} \frac{\partial \eta}{\partial a} + \frac{\partial V}{\partial \delta} \frac{\partial \delta}{\partial a} + \frac{\partial V}{\partial \omega} \frac{\partial \omega}{\partial a}. \quad (71)$$

Therefore to evaluate the axion mass and self-coupling, we need to calculate the 1-4th partial derivatives of each of the physical condensates with respect to a . This can be fulfilled by taking the successive derivatives of the gap equations (67) with respect to a .

III. NUMERICAL RESULTS AND DISCUSSIONS

In this section, we present the numerical results obtained in the NJL model. We focus on the axion potential, axion mass, and axion self coupling at finite T and μ . The properties of axion domain walls in the presence of 2CS are also reported.

We adopt the same model parameters as that in [58], namely $\Lambda = 590$ MeV, $G = 2.435/\Lambda^2$, $c = 0.2$, and $m = 6$ MeV. These parameters are fixed by fitting the physical pion mass, the pion decay constant, and the chiral condensate $\sigma_0 = 2(-241.5 \text{ MeV})^3$ in vacuum. The ratios H_1/G_1 and H_2/G_2 are fixed by the Fierz transformations.

Note that the sensitivities of some results to the variation of c in the range $c = (0, 0.5)$ are also investigated. In addition, the axion mass and self coupling obtained using the ratio H_2/G_2 beyond the the Fierz transformation are given in Appendix.

In the following, the unit MeV in the point (T, μ) is ignored for simplicity.

A. The condensates as functions of a/f_a

In this subsection, we show how the condensates σ , η , δ , and ω vary with the angle $\theta \equiv a/f_a$ at finite temperature and chemical potential.

In Fig.1, we display the chiral condensate σ and diquark condensate δ as functions of μ for several values of

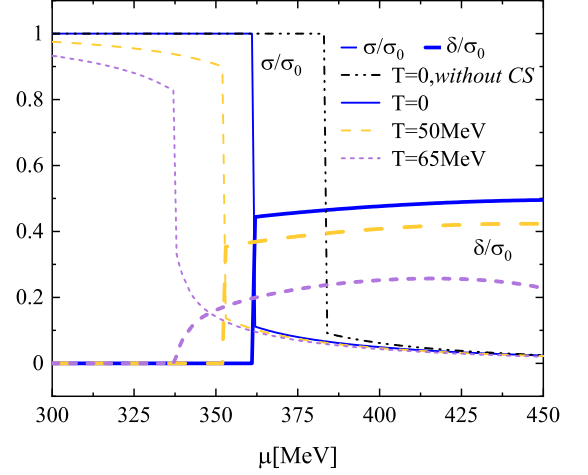


FIG. 1. The chiral condensate σ (thin lines) and diquark condensate δ (bold lines) as functions of μ for several values of T at $a/f_a = 0$. Both condensates are scaled by the vacuum chiral condensate σ_0 . The black dash-dotted-dotted line corresponds to σ at $T = 0$ without considering the CS.

T at $a/f_a = 0$. In this case, the psudo-scalar condensates η and ω are both vanishing. For $T = 0$, the first order chiral transition happens at $\mu \simeq 361, at which σ drops significantly and a finite δ , which corresponds to the gap $\Delta_s = 140, appears. The critical chemical potential at $T = 0$ reduces by $\sim 25 compared to the case without considering the CS (see the dash-dot-dot line). We see that the first order transition is weakened with the increase of T and the 2CS still emerges at $T = 65.$$$$

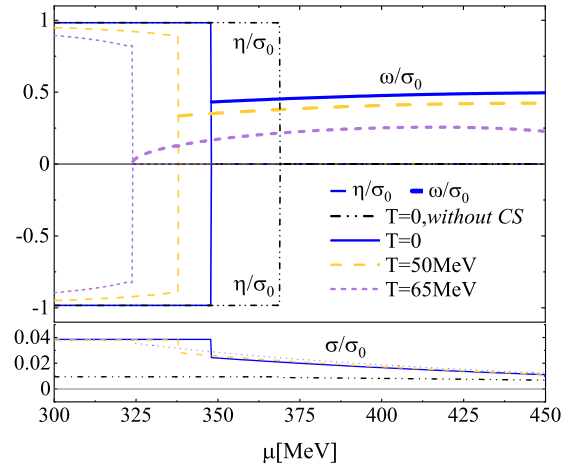


FIG. 2. The condensates σ , η , and ω as functions of μ for several values of T at $a/f_a = \pi$. In the upper panel, the thin (bold) lines refer to η (ω). All the quantities are normalized by σ_0 .

Figure 2 displays σ , η , and ω as functions of μ at $a/f_a = \pi$ for the same values of T as that in Fig.1.

Compared to Fig.1, the roles of the scalar condensate σ (δ) and the pseudo-scalar condensate η (ω) exchange: at lower quark chemical potentials, η dominates and σ becomes very small (but nonzero due to the small quark mass); at larger quark chemical potentials, ω dominates and δ vanishes. This indicates the spontaneous breaking of the parity symmetry for lower temperatures at $a/f_a = \pi$. We notice that η exhibits double values with the same magnitude but opposite sign for $\mu < \mu_c(T)$. This is just the so called Dashen's phenomena[76] characterized by the two-fold vacuum degeneracy at $a/f_a = \pi$. For $\mu > \mu_c(T)$, the η becomes zero and the Dashen's phenomena breaks down, which is similar to the case at finite temperature where Dashen's phenomena only holds for $T < T_c$. Fig.2 shows that at $T = 0$, the η degeneracy is lifted for $\mu > \mu_c = 347$ MeV where η drops to zero and ω appears. In contrast to the case without considering the CS, μ_c is reduced due to the competition between η and ω , which is similar to Fig.1. For higher chemical potential, nonzero ω with vanishing δ corresponds to the solution with $h_L = h_R$ at $a/f_a = \pi$, which is in agreement with the result obtained in [68]. The temperature dependence of ω for fixed $\mu = 350$ and 420 MeV at $a/f_a = \pi$ is displayed in Fig.3.

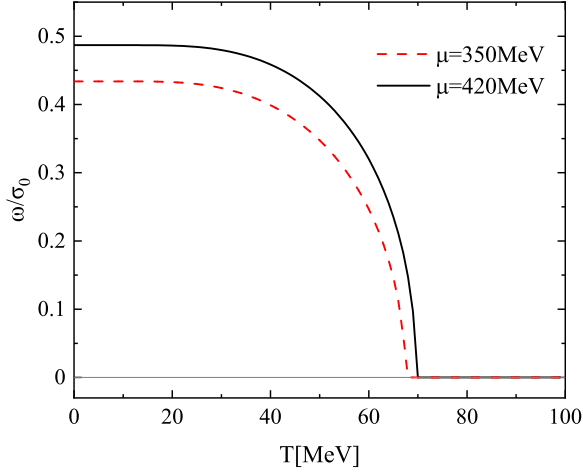


FIG. 3. The normalized pseudo-scalar diquark condensate ω versus T for $\mu = 350$ and 420 MeV at $a/f_a = \pi$.

In Fig.4, we demonstrate σ , η , δ , and ω as functions of θ for several (T, μ) points. The upper panel shows that at $(T, \mu) = (0, 420)$, δ appears but ω vanishes in the θ ranges $(0, \pi/2)$ and $(3\pi/2, 2\pi)$; while in the θ range $(\pi/2, 3\pi/2)$, ω emerges and δ vanishes. This implies a first order phase transition happens at $\theta = \pi/2$ ($3\pi/2$), where the scalar (pseudoscalar) diquark condensate changes into the pseudoscalar (scalar) one. This result is consistent with what obtained in [68]. Similar phase transitions are observed at $(T, \mu) = (0, 365)$ and $(50, 355)$, where diquark condensates are weakened due to the decrease of μ and/or the increase of T . The quark-antiquark condensates σ and η at the same (T, μ) points are displayed in the lower

panel. We see that for the point $(T, \mu) = (0, 420)$ which is a bit far away from the phase boundary at zero θ , the magnitudes of σ and η are obviously less than that of the nonzero δ or ω . For points $(T, \mu) = (0, 365)$ and $(50, 355)$, which are close to the low temperature phase boundary at zero θ , the difference between the quark-antiquark condensates and the non-vanishing diquark condensate δ or ω becomes smaller. In all the three cases, the maximum of the magnitude of ω locates at $\theta = \pi$, where the magnitude of σ becomes smallest and η is zero. Note that the Dashen's phenomenon only appears at (T, μ) points with lower T and μ where the CS does't emerge, as indicated in the lower panel for $(T, \mu) = (60, 320)$.

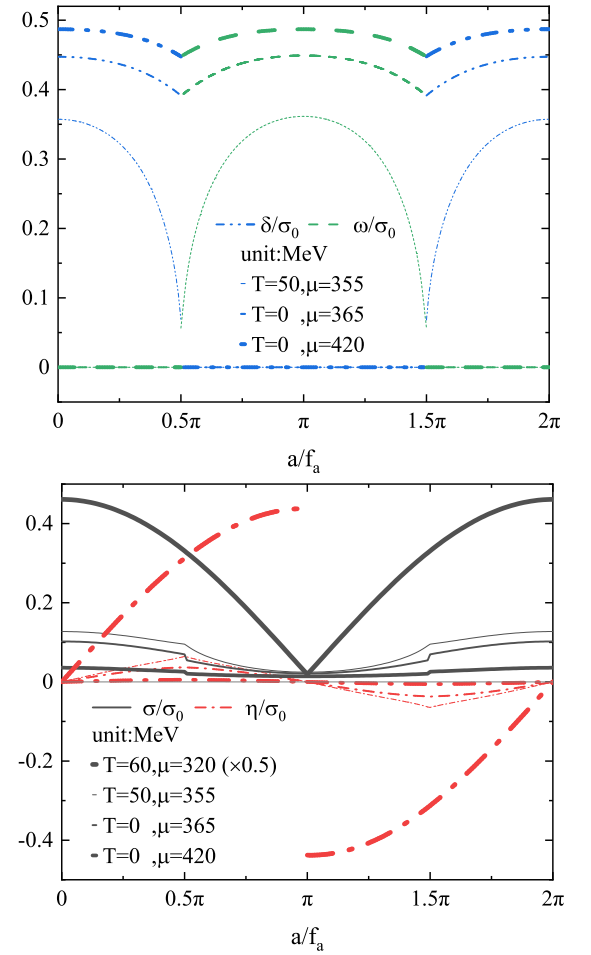


FIG. 4. The normalized diquark condensates δ and ω (upper) and quark-antiquark condensates σ and η (lower) versus $\theta = a/f_a$ for several (T, μ) points. The parameter c is fixed as 0.2.

Figure 5 shows the energy gaps M_s , M_p , Δ_s , and Δ_p versus $\theta = a/f_a$ under the same conditions as that in Fig.4. Since Δ_s and Δ_p contain contributions from both δ and ω , both the gaps form in the whole range $\theta = (0, 2\pi)$. Because Fig.5 is symmetrical about the vertical axis, we only concentrate on the left part of each panel. The upper panel shows Δ_s (Δ_p) de-

creases (increases) with θ in the range $\theta=(0, \pi/2)$ and Δ_p (Δ_s) increases (decreases) in $\theta=(\pi/2, \pi)$. According to Eq.(49), the pseudoscalar Majorana mass becomes $\Delta_p = |2H_2\delta \sin(a/f_a)|$ in $\theta=(0, \pi/2)$ since ω is zero. This formula can be used to explain the behavior of Δ_p in this range: For $(T, \mu)=(0, 420)$, the condensate δ decreases relatively slowly in $\theta=(0, \pi/2)$ (see Fig.4) and thus Δ_p increases with θ in this range as $\sin(a/f_a)$ does; For $(T, \mu)=(50, 355)$, Δ_p first increases and then decreases in $\theta=(0, \pi/2)$ because δ drops rapidly near the left side of $\theta = \pi/2$. The behavior of Δ_s in $\theta=(\pi/2, \pi)$ can be understood in a similar way according to Eq.(48). The lower panel indicates that M_s monotonically decreases with θ up to π , while M_p first increases with θ up to $\pi/2$ and then decreases up to π at which it becomes zero. We see that Δ_s (Δ_p) is much larger than the other three gaps in $\theta = [0, \pi/2]$ ($\theta = [\pi/2, \pi]$) for the two points $(T, \mu)=(0, 420)$ and $(0, 365)$ at zero temperature. But for the point $(T, \mu)=(50, 355)$ with a relatively high temperature, though Δ_s (Δ_p) near $\theta = 0$ (π) is still obviously larger than M_s , it becomes comparable to M_s and M_p around $\theta = \pi/2$ and $3\pi/2$.

B. Axion potential at finite T and μ

The axion potential $V(a, T, \mu) - V(0, T, \mu)$ versus $\theta = a/f_a$ at different (T, μ) points is shown in Fig.6. We see that the behaviors of the axion potential with and without the CS are quite different. For $(T, \mu)=(0, 350)$, the diquark condensate doesn't form and the axion potential exhibits only peak at $\theta = \pi$ in the range $\theta = [0, 2\pi]$. However, for other cases with the 2CS, the axion potential displays two degenerate peaks at $\theta = \pi/2$ and $3\pi/2$ respectively. Moreover, the axion potential at $\theta = \pi$ becomes a local minimum rather than a maximum in the presence of CS. By comparing the cases of $(T, \mu)=(0, 365)$, $(0, 400)$, and $(0, 450)$, we see that the axion potential becomes larger with μ ; by comparing the points of $(T, \mu)=(0, 365)$, $(25, 365)$, and $(50, 365)$, which are close to the phase boundary at zero θ , we observe that the axion potential gets smaller with T .

Figure 6 shows that the axion potential exhibits an approximate periodicity with the period π due to the presence of CS. Such an approximate period turns into an exact one in the chiral limit, as indicated by the blue dotted-line for $(T, \mu)=(0, 400)$. The emergence of the period π is in agreement with the result obtained in [68] where Dirac type masses are not included. Actually, the reason for the period π is the same as that given in [68] since both σ and η are dynamically absent for $m_0 = 0$ in our calculations. In other words, the period π obtained in [68] is broken by the quark masses. We see that such a breaking is quite small at lower temperature and larger quark chemical potential since the axion potentials calculated with and without m_0 are almost coincident. Of course, the breaking becomes relatively obvious near the phase boundary in the T - μ phase diagram because of the

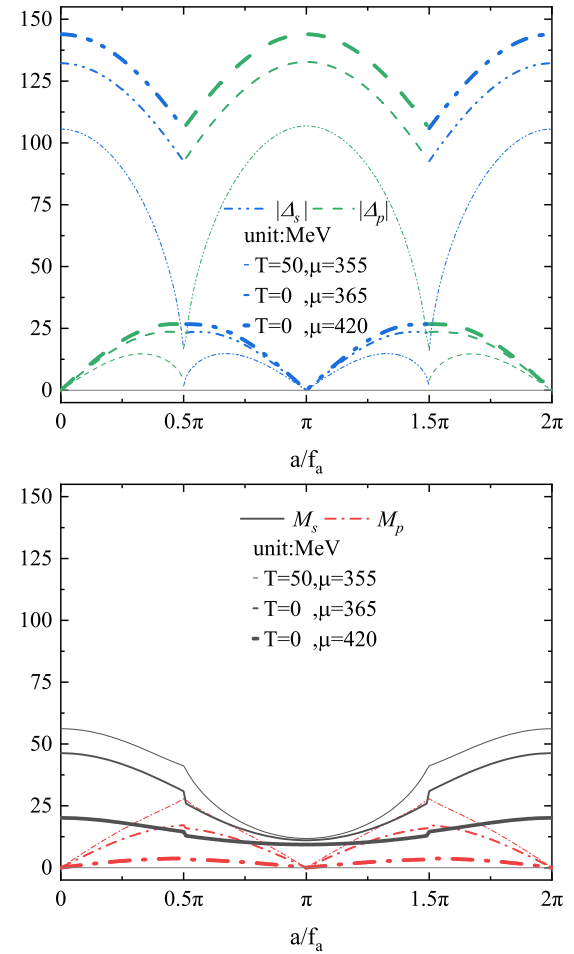


FIG. 5. Majorana masses Δ_s and Δ_p (upper) and Dirac masses M_s and M_p (lower) versus $\theta = a/f_a$. The upper (lower) panel is plotted under the same conditions as that in the upper (lower) panel of Fig.4. The parameter c is fixed as 0.2.

enhanced σ and η , which can be judged by the difference between the axion potentials at $\theta = \pi$ and zero (see the subgraph). We can expect that the breaking of the periodicity with the period π will become more seriously if the coupling constants in diquark channels are weak enough.

C. Topological susceptibility, axion mass, and self-coupling

In this subsection, we present our numerical results on the topological susceptibility, axion mass, and axion self-coupling in the presence of the condensates σ , η , δ , and ω .

The topological susceptibility is a parameter that characterizes the response of QCD vacuum to topological

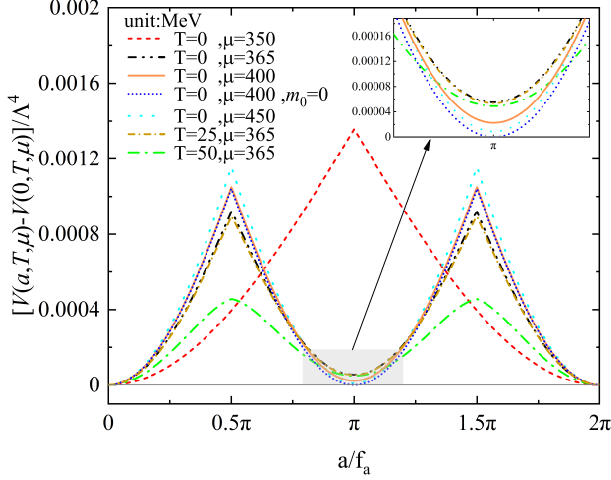


FIG. 6. Axion potential $V(a/f_a, T, \mu) - V(0, T, \mu)$ as functions of $\theta = a/f_a$ for several (T, μ) points. The potential is measured in units of Λ^4 with $\Lambda = 590$ MeV. The parameter c is fixed as 0.2.

charge fluctuations, which is defined as

$$\chi_t = \frac{d^2\Omega}{d\theta^2} \Big|_{\theta=0}. \quad (72)$$

According to Eq.(69), this quantity is proportional to the axion mass squared. The evaluation of χ_t at vacuum and medium has been performed using different non-perturbative methods such as Lattice QCD, chiral perturbation theory and effective models [48, 52, 58].

The calculation of χ_t in the 2CS phase has been given in [68], where an analytical formula has been derived which takes the form

$$\chi_t = H_2 \delta^2 \frac{1 + \frac{H_2}{H_1}}{1 - \frac{H_2}{H_1}} = H_2 \delta^2 (1 - 2c). \quad (73)$$

The rightmost side of (73) is obtained using the relation $H_2/H_1 = G_2/G_1 = c/(1 - c)$, which holds under the assumption that the coupling ratios H_1/G_1 and H_2/G_2 are both limited to the Fierz transformations. Note that the analytical formula (73) doesn't hold when the Dirac masses are considered. Here we mainly focus on how χ_t is affected by the chiral condensate in the presence of the 2CS, especially how it varies across the chiral phase transition line.

In Fig.7, we show the topological susceptibility as functions of μ for different temperatures with $c = 0.2$. For comparison, we also present the results without considering the 2CS and with the 2CS but using the analytical formula (73). We see that before the phase transition, χ_t calculated at zero and low temperatures keeps almost unchanged with $\chi_t^{1/4} \approx 79.8$ MeV, which is close to the standard vacuum value $\chi_t^{1/4} \sim 77.8$ MeV obtained in χ PT theory. At the critical chemical potential, χ_t

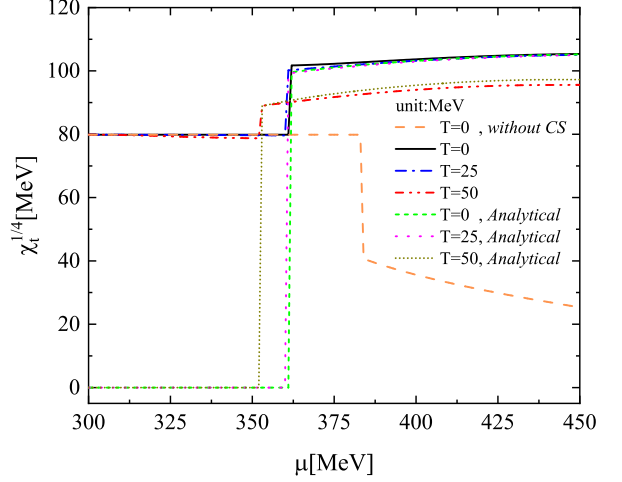


FIG. 7. Topological susceptibility $\chi_t^{1/4}$ versus μ for several values of T . The parameter c is fixed as 0.2.

increases suddenly ($\chi_t^{1/4}$ reaches ~ 100 MeV at $T = 0$) and then grows slowly with μ . This is quite different from the case without including the CS where χ_t drops abruptly at the critical point, as indicated by the long dashed line for $T = 0$. On the other hand, the numerical results of χ_t in the CS phase at $T = 0, 25$ MeV agree quite well with that calculated using the analytical formula for higher μ and small deviations appear near the phase transition point. This suggests that for higher μ and lower T the dominant contribution to χ_t comes from the diquark condensate since the chiral condensate is suppressed significantly. Fig.7 shows that for $T = 50$ MeV, the obvious deviation also emerges at higher μ . This can be attributed to the suppression of the diquark condensate due to the relatively higher T .

Figure 8 displays how χ_t depends on the parameter c . According to Eq.(73), χ_t will become zero for $c = 0.5$. The numerical calculation indicates that χ_t or m_a^2 becomes negative when $c > 0.5$ if μ is large enough. So we only consider the range $c = (0, 0.5)$ (the upper bound 0.5 will be slightly modified for the case with massive quarks.). The upper panel shows that the first order phase transitions with different c almost happen at the same critical chemical potential $\mu_c = 361$ MeV for $T = 0$. The abrupt increase of χ_t due to the emergence of the CS appears in the range $(0.05, 0.45)$: for $\mu < \mu_c$, $\chi_t^{1/4}$ is insensitive to c ; but for $\mu > \mu_c$, it becomes quite sensitive to c . For a very small $c = 0.01$, $\chi_t^{1/4}$ for $\mu < \mu_c$ is obviously less than the standard value 77.8 MeV in vacuum and it further drops in the CS phase. For $c = 0.49$ which is near 0.5, even $\chi_t^{1/4}$ for $\mu < \mu_c$ is still close to the standard vacuum value, it also decreases significantly at the chiral transition point due to the presence of CS. In the lower panel, we show χ_t versus c in the range $c = (0, 0.5)$ for three (T, μ) points near the phase boundary. In the chiral symmetry breaking phase with $(T, \mu) = (0, 360.5)$,

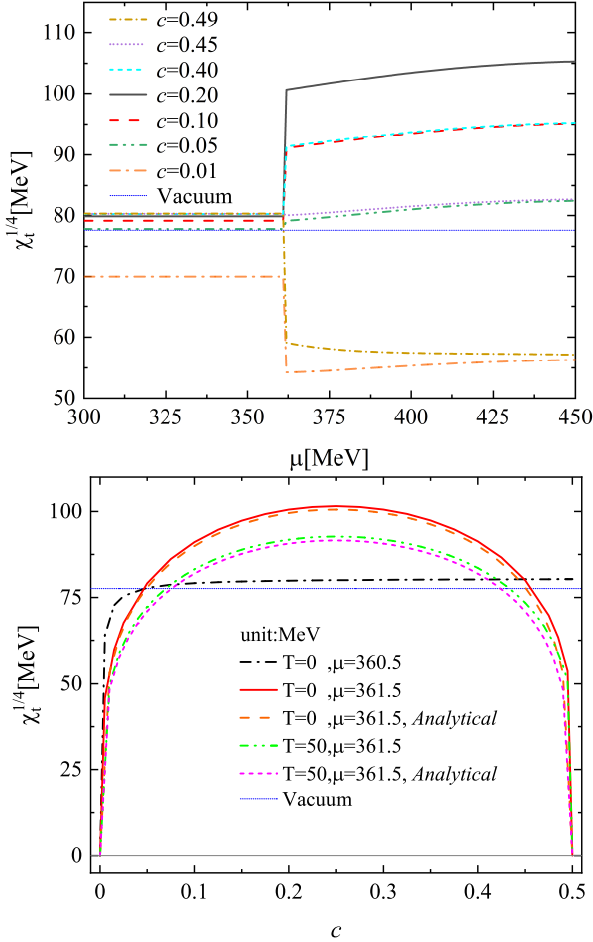


FIG. 8. Upper panel: $\chi_t^{1/4}$ versus μ for several values of c at $T = 0$. Lower panel: $\chi_t^{1/4}$ versus c for several T - μ points in the proximate of the low temperature phase boundary.

the CS doesn't appear and $\chi_t^{1/4}$ keeps almost unchanged for $c > 0.05$; but for $c < 0.05$, it drops obviously with the decreasing of c . In the CS phase with $(T, \mu) = (0, 361.5)$, $\chi_t^{1/4}$ increases with c up to ~ 0.25 and then decreases up to ~ 0.5 . Comparing to its vacuum value, we see that $\chi_t^{1/4}$ become larger in the range $c = (0.05, 0.45)$ for $T = 0$ due to the presence of CS. The similar conclusion is obtained for $T = 50$ MeV where the range of χ_t enhancement due to the CS is shortened. For comparison, we also report $\chi_t^{1/4}$ obtained using the analytic formula (73) in the CS phase for $T = 0, 50$ MeV. We see that the deviation is quite small and thus the analytic formula is still a good approximation for the calculation of χ_t in the presence of σ and δ .

The normalized axion mass as the function of μ under the same conditions as that in Fig.7 and the upper panel of Fig.8 are shown in Figs.9 and 10, respectively. Since the axion mass squared is proportional to χ_t , m_a also rises suddenly at the chiral phase transition point due to the appearance of the CS and then increases with μ if c is not very close to zero or 0.5. This is distinct with the

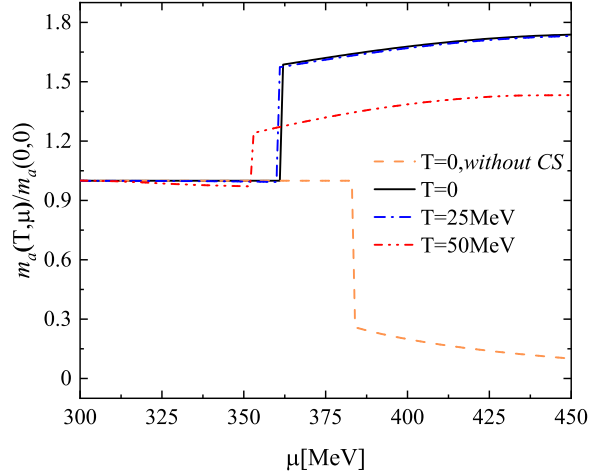


FIG. 9. The normalized axion mass m_a with $c = 0.2$ as a function of μ under the same conditions as that in Fig.7.

case without the CS where m_a decreases obviously at the chiral critical point, as indicated by the long dashed line in Fig.9. Fig.10 displays that for $\mu < \mu_c$ ($\mu > \mu_c$), the normalized m_a is insensitive (sensitive) to c .

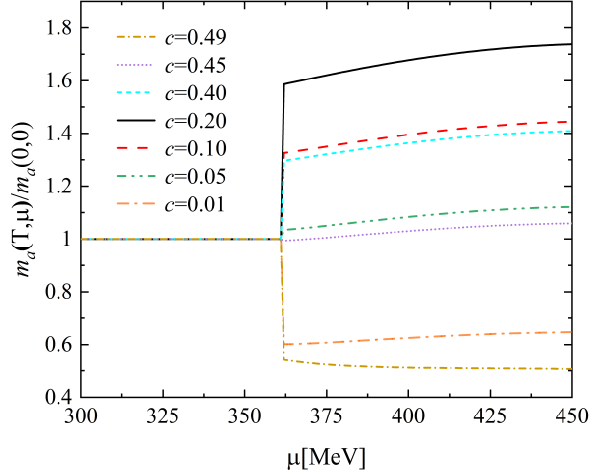


FIG. 10. The axion mass m_a (normalized by its vacuum value obtained using the same c) as a function of μ under the same conditions as that in the upper panel of Fig.8.

The axion self-coupling $\lambda_a(T, \mu)$ (normalized by $\lambda_a(0, 0)$) versus μ for $T = 0, 25, 50$ MeV with $c = 0.2$ is shown in Fig.11. At $T = 0$, the normalized self-coupling rises significantly at μ_c and then decreases with μ . This is quite different from the case without the CS where the normalized self-coupling drops abruptly at the phase transition point, as indicated by the long dashed line. The similar behavior is observed at finite T in the presence of the CS, where the magnitude of $\lambda_a(T, \mu)$ increases with T . In Fig.12, we display the c and μ dependences of $\lambda_a(T, \mu)/\lambda_a(0, 0)$ under the same conditions as that in Fig.8. We see that the μ -dependence

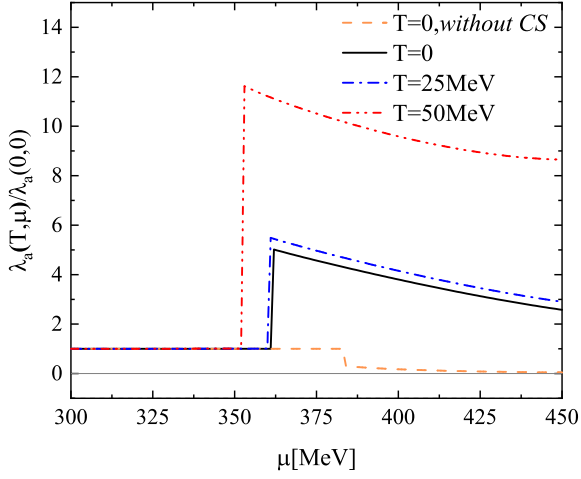


FIG. 11. The normalized axion self-coupling as a function of μ for several values of T with $c = 0.2$.

of the self-coupling is insensitive to c in the chiral symmetry breaking phase but quite sensitive to it in the CS phase. Especially, the self-coupling becomes positive in the range $0.28 < c < 0.50$ ($0.38 < c < 0.50$) at $(T, \mu) = (0, 361.5)$ ($(T, \mu) = (50, 361.5)$). This means that the axion quadratic self-interaction may become repulsive in the 2CS phase if c is large enough. The similar conclusion is also obtained in [68].

The topological susceptibility and the axion self-coupling versus μ at $T = 0$ for different ratios of H_1/G_1 and H_2/G_2 are given in Appendix.

D. The axion domain walls

As shown in Fig.6, the axion potential has two successive vacua at $\theta = 0$ and $\theta = 2\pi$, which permit axion domain wall solution [13] to interpolate between them (details on the domain wall derivation see textbooks [77–79]). The axion domain wall in the medium of dense quark matter without the CS has been explored within the NJL formalism [61]. Here we report our study on properties of axion domain wall in the presence of 2CS.

Following [61], the field equation for the axion $a(x) = f_a \theta(x)$ takes the form

$$\partial_\mu \partial^\mu \theta + \frac{1}{f_a^2} \frac{\partial V(\theta)}{\partial \theta} = 0, \quad (74)$$

where $V(\theta)$ is the axion potential. Eq.(74) has the solitary domain wall solution

$$\theta(x, t) = \theta(x - vt), \quad (75)$$

where v is the propagation speed of the soliton. The field equation can be rewritten as [61]

$$(1 - v^2) \theta_{\xi\xi} = \frac{1}{f_a^2} \frac{\partial V(\theta)}{\partial \theta}, \quad (76)$$

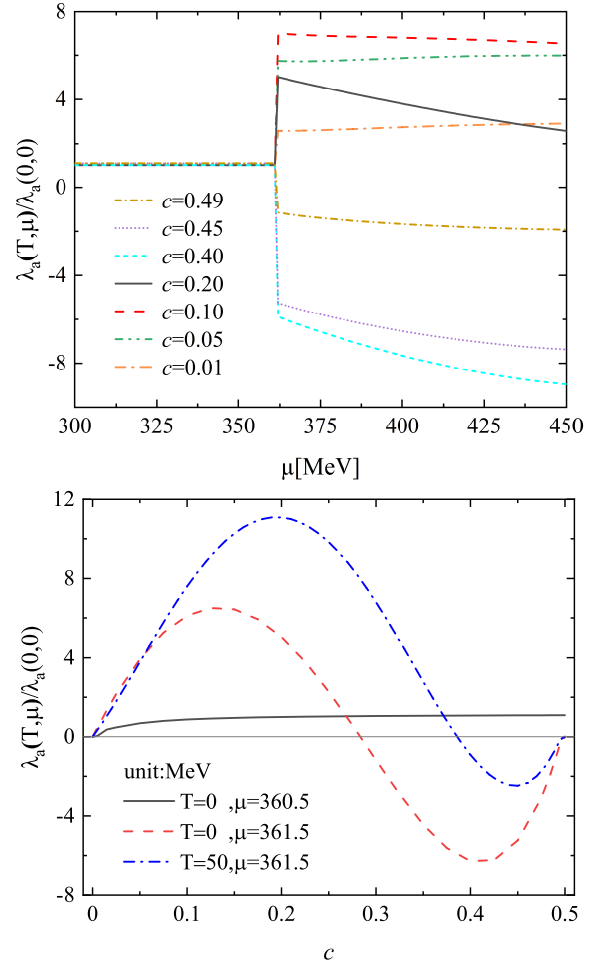


FIG. 12. The normalized axion quadratic self-coupling as functions of μ for several values of c at $T = 0$ (upper) and c at three (T, μ) points (lower). In the lower panel, the chiral symmetry is broken at the point $(T, \mu) = (0, 360.5)$ where the 2CS doesn't appear and restored with the emergence of 2CS at $(T, \mu) = (0, 361.5)$ and $(50, 361.5)$.

where $\xi = x - vt$. Multiplying both sides of Eq.(76) by θ_ξ and integrating with the boundary conditions of $\theta \rightarrow 0$ and $\theta_\xi \rightarrow 0$ for $\xi \rightarrow \pm\infty$, one can obtain the kink and antikink solutions

$$\frac{d\theta}{\sqrt{V(\theta)}} = \pm \sqrt{\frac{2}{f_a^2(1 - v^2)}} d\xi. \quad (77)$$

As in [61], we only consider the soliton at rest and thus we have $x \equiv \xi$. In this case, integrating both sides of (77), one obtains

$$\int_{\pi}^{\theta(x)} \frac{d\theta}{\sqrt{V(\theta)}} = \pm x \sqrt{\frac{2}{f_a^2}}, \quad (78)$$

where the upper limit of the left integration corresponds to the soliton profile $\theta(x)$ which center is required to satisfy $\theta(0) = \pi$. Using an analytical cosine potential (see

the end of this subsection), it has been shown in [61] that the thickness of the axion wall is directly related to the axion mass: the larger the axion mass, the thicker the wall.

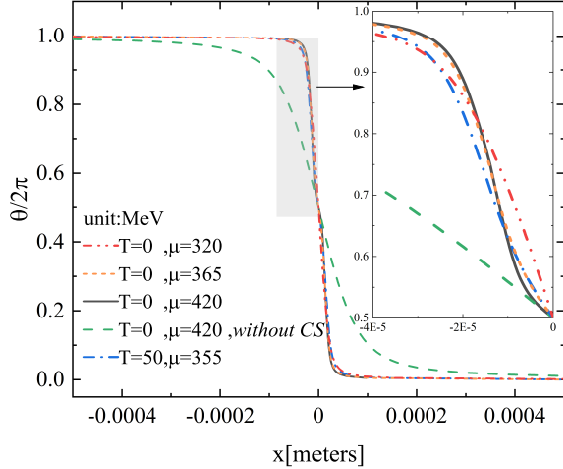


FIG. 13. Axion walls, $\theta = a/f_a$, versus x at different (T, μ) points for $c = 0.2$. $(T, \mu) = (0, 320)$ is a point in the chiral symmetry breaking phase. $(T, \mu) = (0, 365)$, $(50, 355)$ and $(0, 420)$ are three points in the chiral restored phase with the 2CS: the former two (last one) are (is) close to (far from) the phase boundary at $\theta = 0$.

In Fig.13, we plot the axion walls as functions of x at different T and μ . Following [61], $f_a = 10^9 \text{ GeV}$, which is located in the so called classical window, is adopted in the calculations. The red dash-dotted line corresponds to the wall in the chiral symmetry breaking phase at $(T, \mu) = (0, 320)$ and the green dashed line the one in the chiral restored phase without considering the CS at $(T, \mu) = (0, 420)$. The left three lines are the axion walls in the presence of the 2CS which are obtained at $(T, \mu) = (0, 420)$, $(0, 365)$, and $(50, 355)$ respectively. We see that the axion wall in the chiral restored phase without the 2CS is obviously wider than the other four cases. The reason can be traced back to the relatively large axion mass in the 2CS phase or in the chiral symmetry breaking phase. The inset indicates that the wall at $(T, \mu) = (0, 420)$ is narrower than that at $(T, \mu) = (0, 320)$ since the axion mass in the 2CS phase is larger than that in the chiral symmetry breaking phase for $c = 0.2$.

The structure of the center region of the wall for the CS quark matter, namely the four-type condensates and gaps versus x near $x = 0$, are shown in Figs.14 and 15, respectively. Same to Fig.13, the calculations are performed by fixing $f_a = 10^9 \text{ GeV}$. We see that the condensates ω and η form near the core of the wall, which indicates the spontaneous breaking of the parity symmetry. This region has a distinct boundary at which the condensates σ , η , δ , and ω all become discontinuous. In the presence of the 2CS, σ and η are suppressed significantly and ω and δ play dominant roles in the inner and exterior regions of

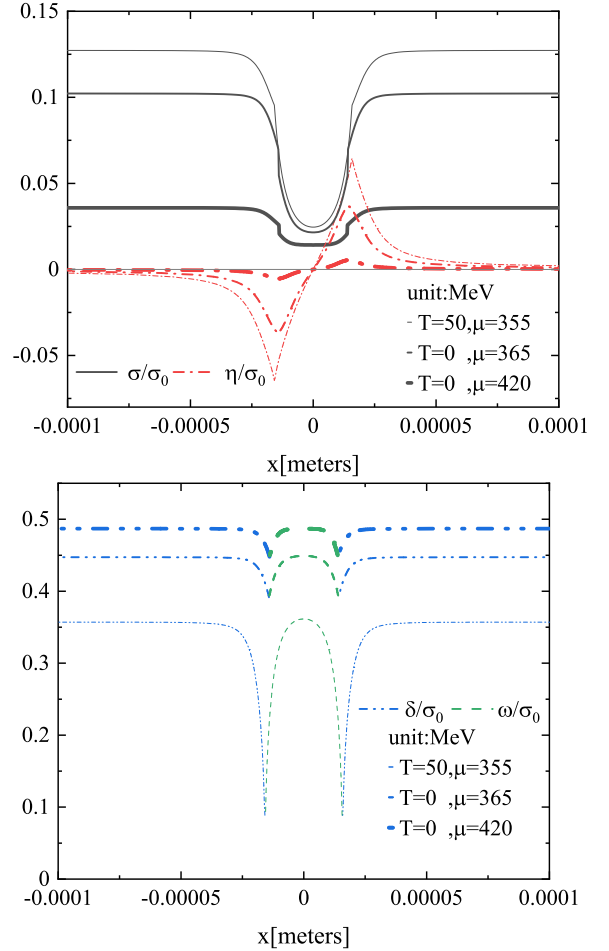


FIG. 14. Axion wall structure: Normalized condensates σ , η (upper), δ , and ω (lower) in the 2CS quark matter versus x for several sets of (T, μ) as in Fig.13 with $c = 0.2$.

the wall, respectively. Analogously, Fig.15 shows that in the core (outside core) region, the gap Δ_p (Δ_s) is much larger than the other gaps.

The surface tension of the domain wall, namely the energy per unit of transverse area, is defined as

$$\kappa = 2\sqrt{2}f_a \int_0^\pi d\theta \sqrt{V(\theta)} \quad (79)$$

for the case with $v = 0$ [52, 61]. This quantity at finite (T, μ) with charge neutrality was first calculated in [61], where the CS was not considered. In Fig.16, we show κ versus μ at $T = 0$ and 50 MeV in the presence of the CS, which is measured by $\kappa_0 = 1.9 \times 10^{16} \text{ MeV}$, the surface tension obtained at $(T, \mu) = (0, 0)$ for $f_a = 10^9 \text{ GeV}$. We see that for $T = 0$, κ/κ_0 decreases from one to ~ 0.85 at the critical chemical potential and then grows slowly with μ . This contrasts with the case without considering the CS where κ/κ_0 drops abruptly from one to ~ 0.20 at the phase transition point, as shown by the solid line. For $T = 50 \text{ MeV}$, the surface tension is weakened in both

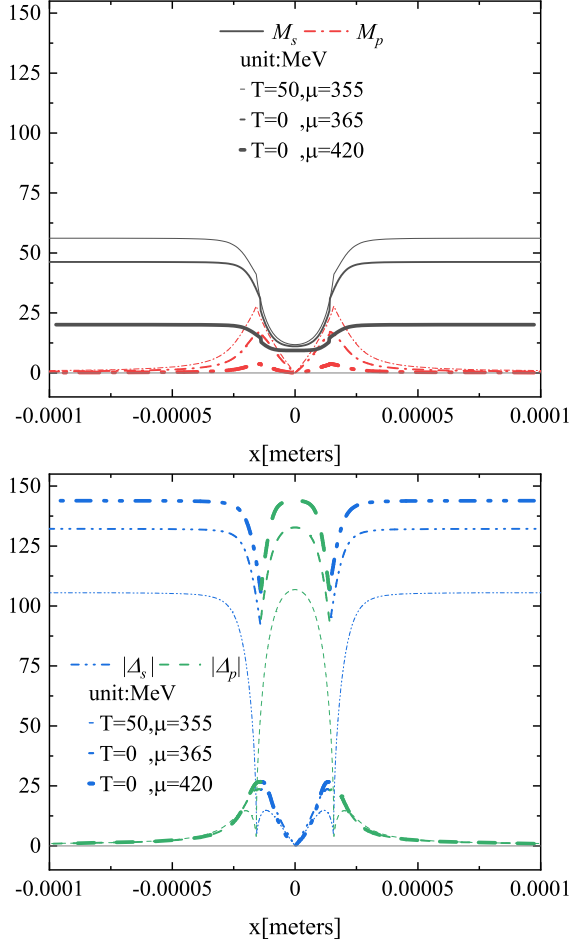


FIG. 15. Axion wall structure: Dirac masses M_s and M_p (upper) and Majorana masses Δ_s and Δ_p (lower) in the 2CS quark matter versus x for several sets of (T, μ) as that in Fig.13 with $c = 0.2$.

the chiral symmetry breaking and CS phases but is still considerable compared to its value at zero T . In addition, Fig.16 shows that the analytic formula

$$\kappa = 8m_a f_a^2 = \frac{8\chi_t}{m_a}, \quad (80)$$

which is obtained by using the simple cosine potential $V(\theta) = m_a^2 f_a^2 (1 - \cos \theta)$ in [61], does not work in the presence of the CS, even it is a very good approximation at larger T/μ for the case without the CS [61].

It has been argued in [61] that forming axion domain walls in the bulk quark matter cost zero energy in the thermodynamic limit. Namely, forming axion walls in bulk quark matter is more easier than forming axion walls in the vacuum. So it might be possible that the axion walls are abundant in the cores of neutron stars. The argument also holds if the bulk quark matter is in the 2CS phase.

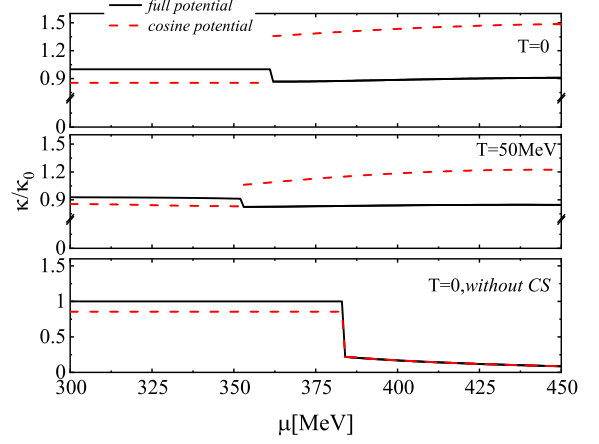


FIG. 16. Dependence of surface tension κ on the quark chemical potential at $T = 0$ and 50 MeV. For comparison, the result at $T = 0$ without considering the CS is also given. This quantity is normalized by $\kappa_0 = 1.9 \times 10^{16} \text{ MeV}^3$, the surface tension obtained in vacuum for $f_a = 10^9 \text{ GeV}$. The parameter c is fixed as 0.2 .

IV. CONCLUSION AND DISCUSSION

We study the QCD axion potential in dense quark matter by simultaneously taking into account the scalar and pseudo-scalar condensates in both the quark-antiquark and diquark channels. We employ the two flavor NJL model with two types of four-quark interactions: one arising from single-gluon exchange and another induced by the instantons. By performing the Fierz transformation, the QCD axion field can be introduced through the instanton induced interactions in both the quark-antiquark and diquark channels in this model. We first obtain the analytic dispersion relations of quarks in the presence of axion field at the mean field level, which involves two scalar condensates σ and δ and two pseudo-scalar condensates η and ω . We then calculate the axion potential, the axion mass (or topological susceptibility), the quadratic self-coupling, and the domain wall tension at finite T/μ . We mainly focus on the influences of the chiral phase transition on these quantities and the effects of Dirac-type masses in the presence of the 2CS.

We found that for larger μ and lower T , the two diquark condensates δ and ω can't exist simultaneously: the former emerges in the ranges $\theta = [0, \pi/2)$ and $(3\pi/2, 2\pi]$, while the latter in the range $\theta = (\pi/2, 3\pi/2)$. Namely, there is a phase transitions at $\theta = \pi/2$ ($3\pi/2$) where δ (ω) drops suddenly to zero. This is consistent with the massless case considered in [68]. In contrast, σ and η can form simultaneously in the CS phase except at $\theta = 0$ and π where η vanishes. We confirmed that the periodicity of the axion potential $V(\theta)$ with a period π found in [68] is disrupted due to the nonzero Dirac masses. However, the axion potential still exhibits double peaks at $\theta = \pi/2$ and $3\pi/2$ and a local minimum at $\theta = \pi$ in the presence of the 2CS: for large enough μ ,

$V(\pi)$ is approaching $V(0)$ and thus π can still be regarded as a good approximate period.

We concluded that the chiral restoration transition doesn't always lead to a reduction of m_a . Instead, the chiral transition with the emergence of the 2CS results in an abrupt increase of m_a for the parameter range $c \approx (0.05, 0.45)$ at $T = 0$. The same conclusion holds for the topological susceptibility since it is proportional to m_a^2 . In addition, the sign and strength of the quadratic self-coupling λ_a in the CS phase are quite sensitive to c . In most of the range $c = (0, 0.5)$, the strength of λ_a is enhanced significantly by the chiral phase transition due to the appearance of 2CS. Moreover, the μ -dependence of $|\lambda_a|$ is also quite sensitive to c .

We confirmed that the width of the domain wall still keeps quite narrow in the chiral symmetric phase with the 2CS at moderate and high μ . Unlike the axion mass, the wall tension in the 2CS phase reduces slightly compared to its value in the chiral symmetry breaking phase at $T = 0$ for $c = 0.2$. This is very different from the case without the 2CS where the wall tension decreases significantly at the chiral phase transition point. We found that the wall tension obtained from the full potential with the 2CS deviates greatly from that calculated using the simple cosine potential.

In this paper, we don't consider the charge neutrality and β -equilibrium constraints which must be taken into account for compact stellar objects such as neutron and protoneutron stars. Our work along this direction is in progress. In addition, it is interesting to investigate the more physical situation with 2+1 flavors by including the strange quark at moderate and high chemical potentials. In this case, more condensates need to be included and the six-fermion interaction induced by the instantons should play a very important role. Furthermore, it is deserved to study the axion effect on the properties of the neutron and protoneutron star where the CS phase may appear in their cores. We leave these topics to future works.

Acknowledgements

This work was supported by the National Natural Science Foundation of China (NSFC) under Grant No. 11875127.

Appendix A: Topological susceptibility and axion self-coupling for different ratios of H_1/G_1 and H_2/G_2

Here we report the numerical calculations on the topological susceptibility (axion mass) and axion self-coupling using the ratios of H_1/G_1 and H_2/G_2 beyond the Fierz transformations.

Figure 17 shows the topological susceptibility $\chi_t^{1/4}$ versus μ for different values of H_1/G_1 and H_2/G_2 at $T = 0$. The parameter c is fixed as 0.2 and $H_1/G_1 = H_2/G_2 = r$ is assumed for simplicity. Fig.17 indicates that $\chi_t^{1/4}$ de-

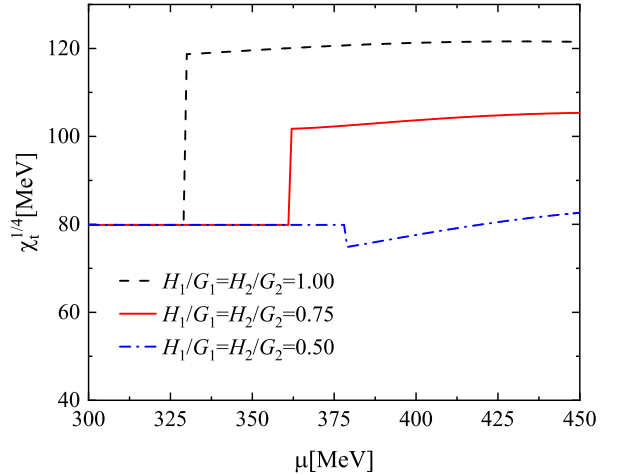


FIG. 17. Topological susceptibility $\chi_t^{1/4}$ versus μ for different ratios of H_1/G_1 and H_2/G_2 at $T = 0$. For simplicity, $H_1/G_1 = H_2/G_2$ is assumed. The parameter c is fixed as 0.2.

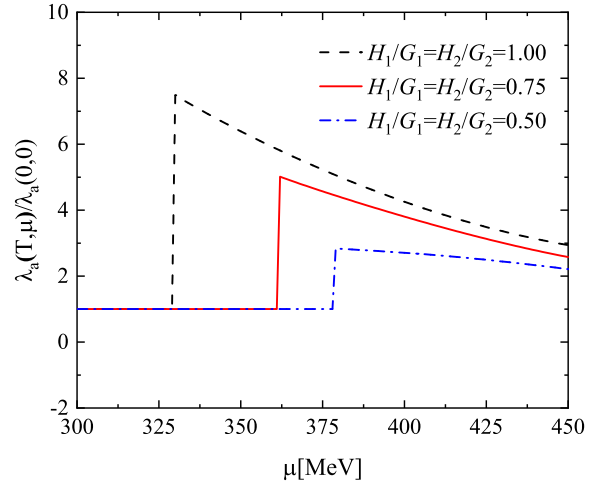


FIG. 18. Normalized axion self-coupling λ_a versus μ under the same conditions as that in Fig.17

creases with the decrease of r in the 2CS phase. For the weaker diquark interactions with $r = 0.5$, χ_t drops at the chiral transition point. But such a decrease is not so significant due to the presence of the 2CS (the gap Δ_s is ~ 70 MeV at $(T, \mu) = (0, 400)$ in this case).

Figure 18 displays the axion self-coupling λ_a versus μ under the same conditions as that in Fig.17. Due to the appearance of the 2CS, the self-coupling gets enhanced at the chiral transition point for all the cases: the stronger the diquark couplings, the more sharply the self-coupling increases at the critical point. Especially for $r = 0.5$, even χ_t declines at the phase transition point, λ_a still increases near threefold.

We also show χ_t and λ_a versus μ for different ratios of H_2/G_2 at $T = 0$ in Figs.19 and 20, respectively, where the parameter c is fixed as 0.2 and $H_1/G_1 = 0.75$ is fixed by the Fierz transformation.

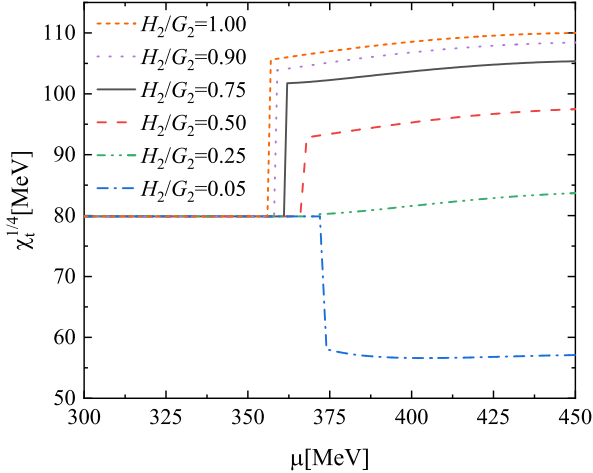


FIG. 19. Topological susceptibility $\chi_t^{1/4}$ versus μ for different ratios of H_2/G_2 at $T = 0$. The parameter c is fixed as 0.2 and $H_1/G_1=0.75$ is fixed by the Fierz transformation.

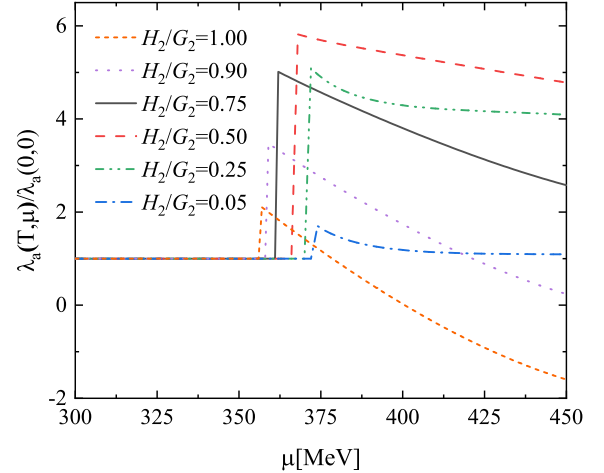


FIG. 20. Normalized axion self-coupling λ_a versus μ under the same conditions as that in Fig.19

[1] R. J. Crewther, P. Di Vecchia, G. Veneziano, and E. Witten. Phys. Lett. B, **88**, 123 (1979). doi:10.1016/0370-2693(79)90128-X

[2] C. A. Baker, D. D. Doyle, P. Geltenbort, K. Green, M. G. D. van der Grinten, P. G. Harris, P. Iaydjiev, S. N. Ivanov, D. J. R. May and J. M. Pendlebury, *et al.* Phys. Rev. Lett. **97**, 131801 (2006) doi:10.1103/PhysRevLett.97.131801 [arXiv:hep-ex/0602020 [hep-ex]].

[3] C. Abel, S. Afach, N. J. Ayres, C. A. Baker, G. Ban, G. Bison, K. Bodek, V. Bondar, M. Burghoff and E. Chanel, *et al.* Phys. Rev. Lett. **124**, no.8, 081803 (2020) doi:10.1103/PhysRevLett.124.081803 [arXiv:2001.11966 [hep-ex]].

[4] R. D. Peccei and H. R. Quinn, Phys. Rev. D **16** (1977), 1791-1797 doi:10.1103/PhysRevD.16.1791

[5] R. D. Peccei and H. R. Quinn, Phys. Rev. Lett. **38**, 1440-1443 (1977) doi:10.1103/PhysRevLett.38.1440

[6] S. Weinberg, Phys. Rev. Lett. **40**, 223-226 (1978) doi:10.1103/PhysRevLett.40.223

[7] F. Wilczek, Phys. Rev. Lett. **40**, 279-282 (1978) doi:10.1103/PhysRevLett.40.279

[8] J. E. Kim and G. Carosi, Rev. Mod. Phys. **82**, 557-602 (2010) [erratum: Rev. Mod. Phys. **91**, no.4, 049902 (2019)] doi:10.1103/RevModPhys.82.557 [arXiv:0807.3125 [hep-ph]].

[9] J. E. Kim, Phys. Rev. Lett. **43** (1979), 103 doi:10.1103/PhysRevLett.43.103

[10] M. A. Shifman, A. I. Vainshtein and V. I. Zakharov, Nucl. Phys. B **166** (1980), 493-506 doi:10.1016/0550-3213(80)90209-6

[11] M. Dine, W. Fischler and M. Srednicki, Phys. Lett. B **104** (1981), 199-202 doi:10.1016/0370-2693(81)90590-6

[12] A. Zhitnitsky, Yad. Fiz.31, 497 (1980); [Sov. J. Nucl. Phys. 31, 260 (1980)].

[13] P. Sikivie, Phys. Rev. Lett. **48** (1982), 1156-1159 doi:10.1103/PhysRevLett.48.1156

[14] J. Preskill, M. B. Wise and F. Wilczek, Phys. Lett. B **120**, 127-132 (1983) doi:10.1016/0370-2693(83)90637-8

[15] L. F. Abbott and P. Sikivie, Phys. Lett. B **120**, 133-136 (1983) doi:10.1016/0370-2693(83)90638-X

[16] M. Dine and W. Fischler, Phys. Lett. B **120**, 137-141 (1983) doi:10.1016/0370-2693(83)90639-1

[17] L. Visinelli and P. Gondolo, Phys. Rev. D **80**, 035024 (2009) doi:10.1103/PhysRevD.80.035024 [arXiv:0903.4377 [astro-ph.CO]].

[18] L. D. Duffy and K. van Bibber, New J. Phys. **11**, 105008 (2009) doi:10.1088/1367-2630/11/10/105008 [arXiv:0904.3346 [hep-ph]].

[19] M. Colpi, S. L. Shapiro and I. Wasserman, Phys. Rev. Lett. **57**, 2485-2488 (1986) doi:10.1103/PhysRevLett.57.2485

[20] I. I. Tkachev, Phys. Lett. B **261**, 289-293 (1991) doi:10.1016/0370-2693(91)90330-S

[21] E. W. Kolb and I. I. Tkachev, Phys. Rev. Lett. **71**, 3051-3054 (1993) doi:10.1103/PhysRevLett.71.3051 [arXiv:hep-ph/9303313 [hep-ph]].

[22] P. H. Chavanis, Phys. Rev. D **84**, 043531 (2011) doi:10.1103/PhysRevD.84.043531 [arXiv:1103.2050 [astro-ph.CO]].

[23] F. S. Guzman and L. A. Urena-Lopez, Astrophys. J. **645**, 814-819 (2006) doi:10.1086/504508 [arXiv:astro-ph/0603613 [astro-ph]].

[24] J. Barranco and A. Bernal, Phys. Rev. D **83**, 043525 (2011) doi:10.1103/PhysRevD.83.043525 [arXiv:1001.1769 [astro-ph.CO]].

[25] E. Braaten, A. Mohapatra and H. Zhang, Phys. Rev. Lett. **117**, no.12, 121801 (2016) doi:10.1103/PhysRevLett.117.121801 [arXiv:1512.00108 [hep-ph]].

[26] S. Davidson and T. Schwetz, Phys. Rev. D **93**, no.12, 123509 (2016) doi:10.1103/PhysRevD.93.123509

[arXiv:1603.04249 [astro-ph.CO]].

[27] J. Eby, M. Leembruggen, P. Suranyi and L. C. R. Wijewardhana, JHEP **12**, 066 (2016) doi:10.1007/JHEP12(2016)066 [arXiv:1608.06911 [astro-ph.CO]].

[28] T. Helfer, D. Marsh, K. Clough, M. Fairbairn, E. Lim, and R. Becerril, J. Cosmol. Astropart. Phys. 03 (2017) 055 doi:10.1088/1475-7516/2017/03/055 [arXiv:1609.04724 [astro-ph.CO]].

[29] D. G. Levkov, A. G. Panin and I. I. Tkachev, Phys. Rev. Lett. **118**, no.1, 011301 (2017) doi:10.1103/PhysRevLett.118.011301 [arXiv:1609.03611 [astro-ph.CO]].

[30] J. Eby, M. Leembruggen, P. Suranyi and L. C. R. Wijewardhana, JHEP **06**, 014 (2017) doi:10.1007/JHEP06(2017)014 [arXiv:1702.05504 [hep-ph]].

[31] L. Visinelli, S. Baum, J. Redondo, K. Freese and F. Wilczek, Phys. Lett. B **777**, 64-72 (2018) doi:10.1016/j.physletb.2017.12.010 [arXiv:1710.08910 [astro-ph.CO]].

[32] P. H. Chavanis, Phys. Rev. D **94**, no.8, 083007 (2016) doi:10.1103/PhysRevD.94.083007 [arXiv:1604.05904 [astro-ph.CO]].

[33] E. Cotner, Phys. Rev. D **94**, no.6, 063503 (2016) doi:10.1103/PhysRevD.94.063503 [arXiv:1608.00547 [astro-ph.CO]].

[34] Y. Bai, V. Barger and J. Berger, JHEP **12**, 127 (2016) doi:10.1007/JHEP12(2016)127 [arXiv:1612.00438 [hep-ph]].

[35] P. Sikivie and Q. Yang, Phys. Rev. Lett. **103**, 111301 (2009) doi:10.1103/PhysRevLett.103.111301 [arXiv:0901.1106 [hep-ph]].

[36] P. H. Chavanis, Phys. Rev. D **98**, no.2, 023009 (2018) doi:10.1103/PhysRevD.98.023009 [arXiv:1710.06268 [gr-qc]].

[37] A. Caputo and G. Raffelt, doi:10.22323/1.454.0041 [arXiv:2401.13728 [hep-ph]].

[38] A. Sedrakian, Phys. Rev. D **93**, no.6, 065044 (2016) doi:10.1103/PhysRevD.93.065044 [arXiv:1512.07828 [astro-ph.HE]].

[39] A. Sedrakian, Phys. Rev. D **99**, no.4, 043011 (2019) doi:10.1103/PhysRevD.99.043011 [arXiv:1810.00190 [astro-ph.HE]].

[40] M. Buschmann, C. Dessert, J. W. Foster, A. J. Long and B. R. Safdi, Phys. Rev. Lett. **128**, no.9, 091102 (2022) doi:10.1103/PhysRevLett.128.091102 [arXiv:2111.09892 [hep-ph]].

[41] L. B. Leinson, JCAP **08**, 031 (2014) doi:10.1088/1475-7516/2014/08/031 [arXiv:1405.6873 [hep-ph]].

[42] R. Balkin, J. Serra, K. Springmann, S. Stelzl and A. Weiler, [arXiv:2211.02661 [hep-ph]].

[43] B. S. Lopes, R. L. S. Farias, V. Dexheimer, A. Bandyopadhyay and R. O. Ramos, Phys. Rev. D **106**, no.12, L121301 (2022) doi:10.1103/PhysRevD.106.L121301 [arXiv:2206.01631 [hep-ph]].

[44] G. Lucente, P. Carenza, T. Fischer, M. Giannotti and A. Mirizzi, JCAP **12**, 008 (2020) doi:10.1088/1475-7516/2020/12/008 [arXiv:2008.04918 [hep-ph]].

[45] T. Fischer, P. Carenza, B. Fore, M. Giannotti, A. Mirizzi and S. Reddy, Phys. Rev. D **104**, no.10, 103012 (2021) doi:10.1103/PhysRevD.104.103012 [arXiv:2108.13726 [hep-ph]].

[46] D. Noordhuis, A. Prabhu, C. Weniger and S. J. Witte, Phys. Rev. X **14**, no.4, 041015 (2024) doi:10.1103/PhysRevX.14.041015 [arXiv:2307.11811 [hep-ph]].

[47] E. Berkowitz, M. I. Buchoff and E. Rinaldi, Phys. Rev. D **92**, no.3, 034507 (2015) doi:10.1103/PhysRevD.92.034507 [arXiv:1505.07455 [hep-ph]].

[48] S. Borsanyi, Z. Fodor, J. Guenther, K. H. Kampert, S. D. Katz, T. Kawanai, T. G. Kovacs, S. W. Mages, A. Pasztor and F. Pittler, *et al.* Nature **539**, no.7627, 69-71 (2016) doi:10.1038/nature20115 [arXiv:1606.07494 [hep-lat]].

[49] S. Aoki *et al.* [JLQCD], EPJ Web Conf. **175**, 04008 (2018) doi:10.1051/epjconf/201817504008 [arXiv:1712.05541 [hep-lat]].

[50] C. Bonati, M. D’Elia, M. Mariti, G. Martinelli, M. Mesiti, F. Negro, F. Sanfilippo and G. Villadoro, JHEP **03**, 155 (2016) doi:10.1007/JHEP03(2016)155 [arXiv:1512.06746 [hep-lat]].

[51] P. Petreczky, H. P. Schadler and S. Sharma, Phys. Lett. B **762**, 498-505 (2016) doi:10.1016/j.physletb.2016.09.063 [arXiv:1606.03145 [hep-lat]].

[52] G. Grilli di Cortona, E. Hardy, J. Pardo Vega and G. Villadoro, JHEP **01**, 034 (2016) doi:10.1007/JHEP01(2016)034 [arXiv:1511.02867 [hep-ph]].

[53] Y. Nambu and G. Jona-Lasinio, Phys. Rev. **122**, 345-358 (1961) doi:10.1103/PhysRev.122.345

[54] Y. Nambu and G. Jona-Lasinio, Phys. Rev. **124**, 246-254 (1961) doi:10.1103/PhysRev.124.246

[55] S. P. Klevansky, Rev. Mod. Phys. **64**, 649-708 (1992) doi:10.1103/RevModPhys.64.649

[56] T. Hatsuda and T. Kunihiro, Phys. Rept. **247**, 221-367 (1994) doi:10.1016/0370-1573(94)90022-1 [arXiv:hep-ph/9401310 [hep-ph]].

[57] M. Buballa, Phys. Rept. **407**, 205-376 (2005) doi:10.1016/j.physrep.2004.11.004 [arXiv:hep-ph/0402234 [hep-ph]].

[58] Z. Y. Lu and M. Ruggieri, Phys. Rev. D **100**, no.1, 014013 (2019) doi:10.1103/PhysRevD.100.014013 [arXiv:1811.05102 [hep-ph]].

[59] A. Bandyopadhyay, R. L. S. Farias, B. S. Lopes and R. O. Ramos, Phys. Rev. D **100**, no.7, 076021 (2019) doi:10.1103/PhysRevD.100.076021 [arXiv:1906.09250 [hep-ph]].

[60] A. Abhishek, A. Das, H. Mishra and R. K. Mohapatra, Phys. Rev. D **103**, no.7, 074003 (2021) doi:10.1103/PhysRevD.103.074003 [arXiv:2006.15727 [hep-ph]].

[61] B. Zhang, D. E. A. Castillo, A. G. Grunfeld and M. Ruggieri, Phys. Rev. D **108**, no.5, 054010 (2023) doi:10.1103/PhysRevD.108.054010 [arXiv:2304.10240 [hep-ph]].

[62] M. G. Alford, K. Rajagopal and F. Wilczek, Phys. Lett. B **422**, 247-256 (1998) doi:10.1016/S0370-2693(98)00051-3 [arXiv:hep-ph/9711395 [hep-ph]].

[63] R. Rapp, T. Schäfer, E. V. Shuryak and M. Velkovsky, Phys. Rev. Lett. **81**, 53-56 (1998) doi:10.1103/PhysRevLett.81.53 [arXiv:hep-ph/9711396 [hep-ph]].

[64] M. G. Alford, K. Rajagopal and F. Wilczek, Nucl. Phys. B **537**, 443-458 (1999) doi:10.1016/S0550-3213(98)00668-3 [arXiv:hep-ph/9804403 [hep-ph]].

[65] R. Rapp, T. Schäfer, E. V. Shuryak and

M. Velkovsky, Annals Phys. **280**, 35-99 (2000) doi:10.1006/aphy.1999.5991 [arXiv:hep-ph/9904353 [hep-ph]].

[66] M. G. Alford, A. Schmitt, K. Rajagopal and T. Schäfer, Rev. Mod. Phys. **80**, 1455-1515 (2008) doi:10.1103/RevModPhys.80.1455 [arXiv:0709.4635 [hep-ph]].

[67] R. Balkin, J. Serra, K. Springmann and A. Weiler, JHEP **07**, 221 (2020) doi:10.1007/JHEP07(2020)221 [arXiv:2003.04903 [hep-ph]].

[68] F. Murgana, D. E. A. Castillo, A. G. Grunfeld and M. Ruggieri, Phys. Rev. D **110**, no.1, 014042 (2024) doi:10.1103/PhysRevD.110.014042 [arXiv:2404.14160 [hep-ph]].

[69] T. Hatsuda, M. Tachibana, N. Yamamoto and G. Baym, Phys. Rev. Lett. **97**, 122001 (2006) doi:10.1103/PhysRevLett.97.122001 [arXiv:hep-ph/0605018 [hep-ph]].

[70] Z. Zhang, K. Fukushima and T. Kunihiro, Phys. Rev. D **79**, 014004 (2009) doi:10.1103/PhysRevD.79.014004 [arXiv:0808.0927 [hep-ph]].

[71] Z. Zhang and T. Kunihiro, Phys. Rev. D **80**, 014015 (2009) doi:10.1103/PhysRevD.80.014015 [arXiv:0904.1062 [hep-ph]].

[72] Z. Zhang and T. Kunihiro, Eur. Phys. J. A **52**, no.8, 230 (2016) doi:10.1140/epja/i2016-16230-y [arXiv:1510.04417 [hep-ph]].

[73] S. B. Ruester, V. Werth, M. Buballa, I. A. Shovkovy and D. H. Rischke, Phys. Rev. D **72**, 034004 (2005) doi:10.1103/PhysRevD.72.034004 [arXiv:hep-ph/0503184 [hep-ph]].

[74] D. Blaschke, S. Fredriksson, H. Grigorian, A. M. Oztas and F. Sandin, Phys. Rev. D **72**, 065020 (2005) doi:10.1103/PhysRevD.72.065020 [arXiv:hep-ph/0503194 [hep-ph]].

[75] J. I. Kapusta and C. Gale, “Finite-Temperature Field Theory,” Cambridge University Press, 2023, ISBN 978-1-009-40196-8, 978-1-009-40195-1, 978-1-009-40198-2 doi:10.1017/9781009401968

[76] R. F. Dashen, Phys. Rev. D **3**, 1879 (1971)

[77] M. Shifman, *Advanced Topics in Quantum Field Theory*, Cambridge University Press, 2022, ISBN 978-1-108-88591-1, 978-1-108-84042-2 doi:10.1017/9781108885911

[78] E. J. Weinberg, Cambridge University Press, 2012, ISBN 978-0-521-11463-9, 978-1-139-57461-7 doi:10.1017/CBO9781139017787

[79] Y. Nagashima, *Beyond the standard model of elementary particle physics*, Wiley-VCH, 2014, ISBN 978-3-527-41177-1, 978-3-527-66505-1